Multidimensional Isotropic Magnetic Shielding Contour Maps for the Visualization of Aromaticity in *ortho*-Arynes and Their Reactions

Albert Artigas
Denis Hagebaum-Reignier
Yannick Carissan*
Yoann Coquerel*

Aix-Marseille Univ, CNRS, Centrale Marseille, iSm2, Marseille, France
yannick.carissan@univ-amu.fr
yoann.coquerel@univ-amu.fr

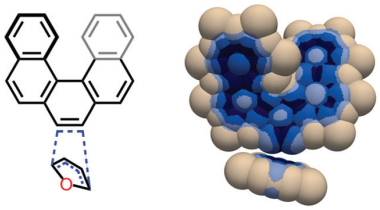

Abstract Visualization of electron delocalization and aromaticity in some selected arynes, including nonplanar examples, and their Diels–Alder or dimerization reactions was achieved through multidimensional isotropic magnetic shielding contour maps. These maps showed that arynes are generally less aromatic than the corresponding arenes, and that aromaticity peaks during their reactions when approaching the transition state.

Key words arynes, aromaticity, DFT calculations, contorted molecules

ortho-Arynes, herein referred to as arynes, are important tools in synthetic organic chemistry for the synthesis of partially or fully aromatic molecules. The synthesis of some complex natural products was enabled by arynes,[1] and they have also proven useful for the synthesis of large polycyclic aromatic hydrocarbon molecules.[2] Arynes are electrophilic reaction intermediates that easily undergo addition reactions with nucleophiles, and cycloaddition reactions with unsaturated molecules. Arynes are strained short-lived species that must be generated in situ, usually through the *ortho*-elimination of a suitable aromatic precursor.[3]

Previous theoretical analyses of the electronic structure and aromaticity of benzyne (**1**) using magnetic criteria showed that it is aromatic and better described as an acetylene- rather than a cumulene-containing molecule.[4] Magnetics in a few other arynes were also investigated, which led to comparable conclusions.[5] It should, however, be kept in mind that the traditional Lewis structure of arynes with a triple bond is an oversimplification of their electronic structure. Electronically, planar arynes have two distinct π-systems that do not overlap: a 6π [or more generally a (4n+2)π]-aromatic system made of six (or more) overlapping *p*-orbitals as in benzene (or larger polycyclic aromatic hydrocarbons), and a 2π-reacting system oriented in the molecular plane, perpendicularly to the aromatic π-system, made of two weakly overlapping sp^2-resembling orbitals. This weak overlap is, in part, responsible for the high chemical reactivity of arynes.

The calculation of nucleus independent chemical shift (NICS) provides an indirect yet reliable evaluation of aromaticity in molecules.[6] Isotropic magnetic shielding (IMS or σ_{iso}) is the negative of isotropic NICS calculations [IMS = $-NICS_{iso} = (\sigma_{xx} + \sigma_{yy} + \sigma_{zz}) / 3$]. It averages properties in the three directions of space and can be applied to any molecular system independently of the spatial arrangement of its atoms. Herein, it is proposed to visualize electron delocalization and aromaticity in benzyne and three larger arynes, including contorted ones, using 2D[7] or 3D[8] isotropic magnetic shielding (IMS) contour maps. The variations in aromaticity during some archetypal cycloaddition reactions of these arynes were also examined. The resulting contour maps of electron delocalization provided pictorial intuitive yet detailed and quantitative evaluation of (anti)aromaticity in arynes and their reactions.

All calculations were performed with the Gaussian 16 package.[9] Optimizations of geometries were performed in the gas phase without symmetry constraints using the M06-2X-D3(0)/cc-pVDZ level of theory for the results in Figure 1, Figure 3, and Figure 4, and using the UM06-2X-D3(0)/cc-pVDZ level of theory for the results in Figure 2.[10,11] The corresponding .xyz files are provided as Supporting Information. Analytical Hessians were computed to confirm that the optimized geometries are indeed minima (zero imaginary frequency) or transition states (one imaginary frequency). NMR-GIAO[12] calculations of IMS were performed at the (U)B3LYP-GIAO/6-311++G(d,p)[13] level of theory. The 2D IMS contour maps were generated in a plane located 1 Å above the mean plane defined by the C atoms of

the considered aromatic system,[7] while 3D IMS contour maps were generated on a surface made of 1 Å radius spheres around all atoms, including some artificially introduced dummy atoms at specific locations.[8] Interpretation of the 2D and 3D IMS contour maps is intuitive: color becomes darker with an increase of the absolute value of IMS with blue indicating an aromatic character (positive IMS), and red indicating an antiaromatic character (negative IMS). Dark blue rings indicate plain aromaticity as in benzene (see example in Figure 1, a). The 3D IMS contour maps are interactive and are available for visualization (and personalization) in the Supporting Information as .vtk files. The reader is encouraged to take full advantage of this (see a tutorial in reference 8).

The 2D IMS contour maps of benzene and benzyne (**1**) were first generated (Figure 1, a). In agreement with previous analyses, the map of benzene shows a dark blue circle reminiscent of a Clar π-sextet,[14] while the map of benzyne (**1**) shows a discontinuous dark blue area accounting for less delocalization of its six-electron π-system indicating a comparatively weaker aromatic character. Considering that benzyne (**1**) can also be regarded as a singlet biradical,[15] its 2D IMS contour map was also generated using unrestricted calculations and found to be very comparable with the map of **1** in Figure 1, a (see Supporting Information, Figure S1, a). As the benchmark reaction, we examined the [4+2] cycloaddition between benzyne (**1**) and furan (Figure 1, b). This cycloaddition was computed as a concerted and synchronous transformation with the two new C–C bonds forming simultaneously,[16] which allowed the identification of three stationary points: the reactant complex **1-furan_rc**, the transition state **1-furan_ts**, and the product **1-furan_pro** (Figure 1, c). The 2D IMS contour maps of these three stationary points were computed to visualize the variations in aromaticity during this reaction. The map of **1-furan_rc** showed that the benzyne six-membered ring in the reactant complex is more aromatic than in benzyne itself. The map of **1-furan_ts** indicated a further increase in the aromaticity of this ring, making the transition state the most aromatic species of the overall transformation. This result agrees well with earlier conclusions on the aromatic character of the transition state in the Bergman cyclization of (*Z*)-hexa-1,5-diyn-3-ene affording *para*-benzyne.[4b] Finally, the map of **1-furan_pro** revealed an aromatic character of the product, albeit reduced when compared to benzene.

Next, the recently reported regioselective dimerization of 1,2-benzo[*c*]phenanthryne (**2**) through a (2+2) annulation was examined (Figure 2).[17] Aryne **2** is a peculiar aryne. Its precursors and reaction products are helically twisted in their most stable conformations,[17,18] but aryne **2** itself is a planar compound due to the absence of a hydrogen atom at position 1, resulting in no significant repulsive van der

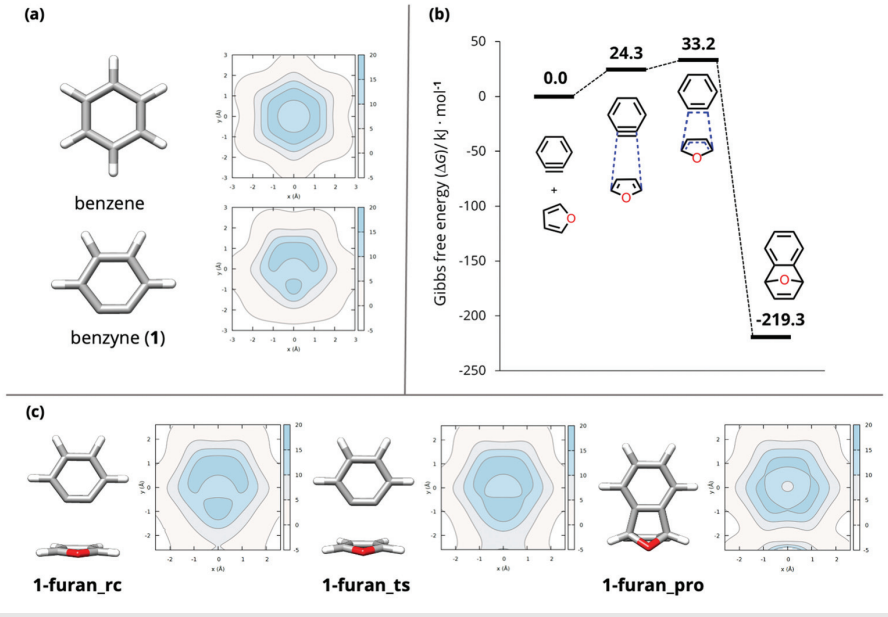

Figure 1 (a) 2D IMS contour maps of benzene and benzyne (**1**). (b) Gibbs free-energy profile of the [4+2] cycloaddition between benzyne (**1**) and furan (results obtained from reference 16 and re-computed for homogeneity). Electronic energies (*E*) are provided in the Supporting Information (Figure S1, b). Relaxed scan between the reactant complex and the separated substrates showed the first step is a barrierless process. (c) 2D IMS contour maps of the three stationary points identified in (b); analysis was performed in the plane located 1 Å above the aromatic six-membered ring on the side of the oxygen atom, that is in front of the depicted systems.

Waals interactions. Because of this, it was decided to visualize delocalization and (anti)aromaticity in aryne **2** by a 2D IMS contour map, while 3D maps were employed to examine (anti)aromaticity during its dimerization. Examination of the map of aryne **2** shows different delocalization patterns at the two terminal rings, revealing less delocalization in the dedihydrogenated reactive ring **2** (Figure 2, a), a situation comparable to benzyne (**1**) *vs* benzene in Figure 1. The dimerization of aryne **2** leading to the helically twisted dimer **2-dimer_pro** was earlier computed as a stepwise process in which London dispersion is governing the regioselectivity.[17] Formation of the C2–C2′ bond occurs first through a barrierless dimerization affording the biradical intermediate **2-dimer_int**, and the latter then undergoes rotation around the newly formed C(sp^2)–C(sp^2) single bond through the transition state **2-dimer_ts** and cyclization to give the product **2-dimer_pro** (Figure 2, b). In the map of intermediate **2-dimer_int**, there is no visible conjugation between the two tetracyclic units as indicated by the neutral color over the C(sp^2)–C(sp^2) single bond (Figure 2, c). As for the cycloaddition examined in Figure 1, the rotation transition state **2-dimer_ts** is seemingly the most aromatic species of the reaction though the effect is little in this case. The (2+2) dimer **2-dimer_pro** contains a four-membered cyclobutadiene ring at its core. This ring contains four conjugated π-electrons and is Hückel antiaromatic. The local antiaromatic character of the cyclobutadiene ring is clearly rendered in the corresponding map with a dark red color area in the middle of this ring and a reduced aromatic character of the two vicinal six-membered rings.

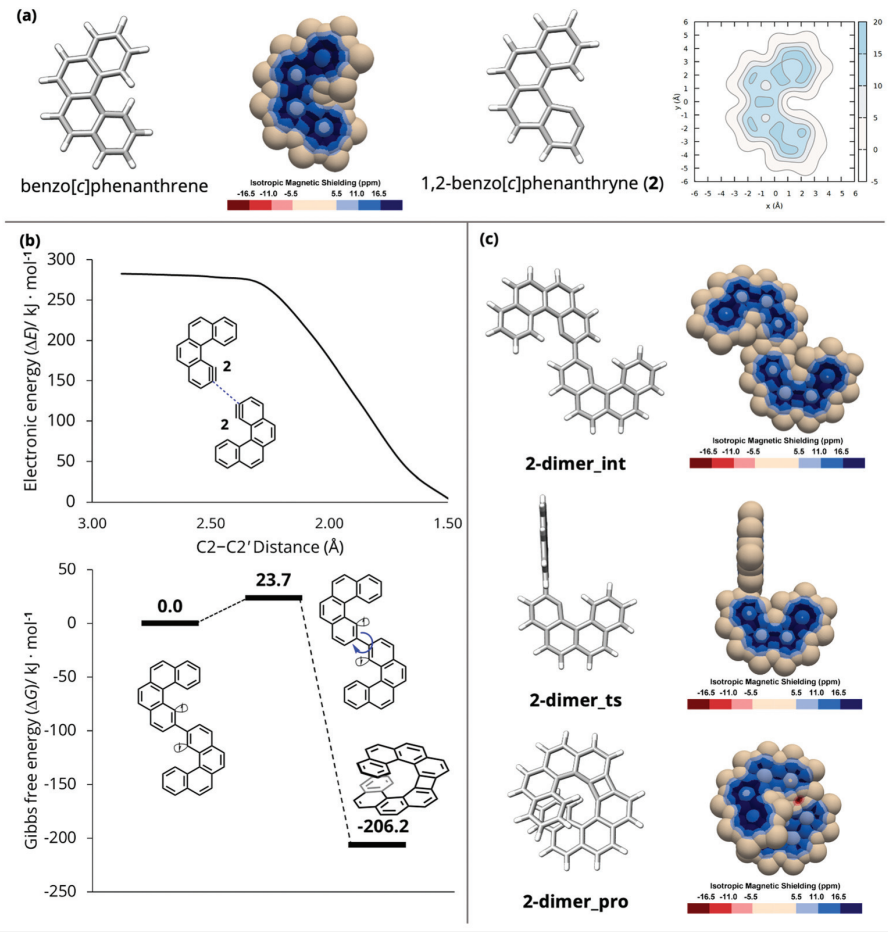

Figure 2 (a) 3D IMS contour map of benzo[c]phenanthrene and 2D IMS contour map of 1,2-benzo[c]phenanthryne (**2**). The 3D IMS contour map of 1,2-benzo[c]phenanthryne (**2**) is provided in the Supporting Information for comparison. (b) Relaxed scan of the C2–C2′ distance showing a barrierless formation of **2-dimer_int**, and Gibbs free-energy profile of the annulation step leading to **2-dimer_pro** (results obtained from reference 17 and recomputed for homogeneity). Electronic energies (*E*) are provided in the Supporting Information (Figure S2). (c) 3D IMS contour maps of the three stationary points identified in (b).

The next examined aryne was 7,8-[5]helicyne (**3**), a contorted aryne with a torsion (that is, the maximal dihedral angle between two nonadjacent C–C bonds in the aryne six-membered ring) of 9.9° (Figure 3).[19] One consequence of the torsion in aryne **3** is that its aromatic π-system and its reactive 2π-system are no longer perpendicular and overlap to some degree. Also, the σ- and π-systems are no longer strictly separated and overlap to some extent. Analysis of π-electron delocalization in contorted molecules is not straightforward. Visualization of electron delocalization in the contorted aryne **3** was realized through 3D IMS contour maps (Figure 3). As for benzyne (**1**) and 1,2-benzo[*c*]phenanthryne (**2**), 7,8-[5]helicyne (**3**) shows some localized character of the π-electrons around the triple bond when compared to [5]helicene (Figure 3, a). The [4+2] cycloaddition of aryne **3** with furan afforded the corresponding cycloadduct **3-furan_pro** in good yield.[19b] Modeling of this reaction by DFT methods revealed a concerted asynchronous process through the transition state **3-furan_ts** (Figure 3, b), contrasting with the synchronous mechanism identified for the reaction of benzyne (**1**) with furan (Figure 1). This difference may be attributed to the torsion in aryne **3**. The maps of the reactant complex **3-furan_rc** and the transition state **3-furan_ts** are comparable with a slightly augmented delocalization prior to bond formation in **3-furan_ts** (Figure 3, c). The map of the cycloadduct **3-furan_pro** shows a delocalization pattern comparable with the one in [5]helicene.

Finally, aromaticity in corannulyne (**4**),[20] another kind of contorted aryne showing a torsion of 10.0°, was examined (Figure 4, a). A comparison of its 3D IMS contour map (both faces) with the map of corannulene[21] is consistent with the previous observations, showing a more localized character of the π-electrons around the triple bond in corannulyne (**4**). The [4+2] cycloaddition of corannulyne (**4**) with anthracene afforded the corresponding cycloadduct **4-anthracene_pro**,[20b] and modeling of this cycloaddition revealed a concerted synchronous process through the transition state **4-anthracene_ts** (Figure 4, b). The transition state **4-anthracene_ts** is the most aromatic species of the

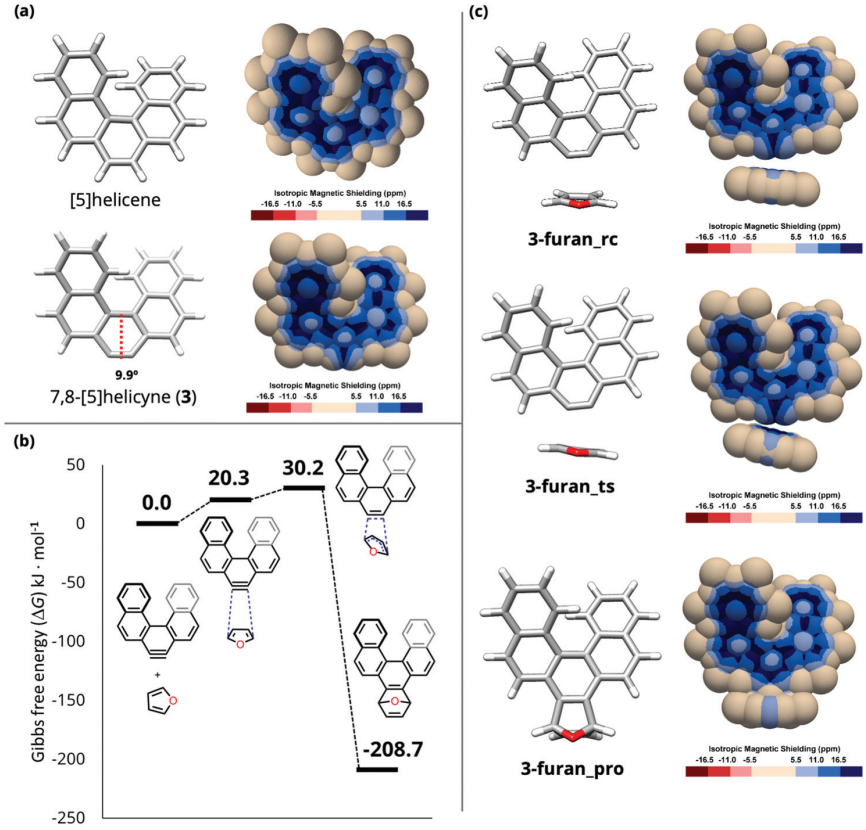

Figure 3 (a) 3D IMS contour maps of [5]helicene and 7,8-[5]helicyne (**3**). (b) Gibbs free-energy profile of the [4+2] cycloaddition between 7,8-[5]helicyne (**3**) and furan. Electronic energies (*E*) are provided in the Supporting Information (Figure S3). Relaxed scan between the reactant complex and the separated substrates showed the first step is a barrierless process. (c) 3D IMS contour maps of the three stationary points identified in (b).

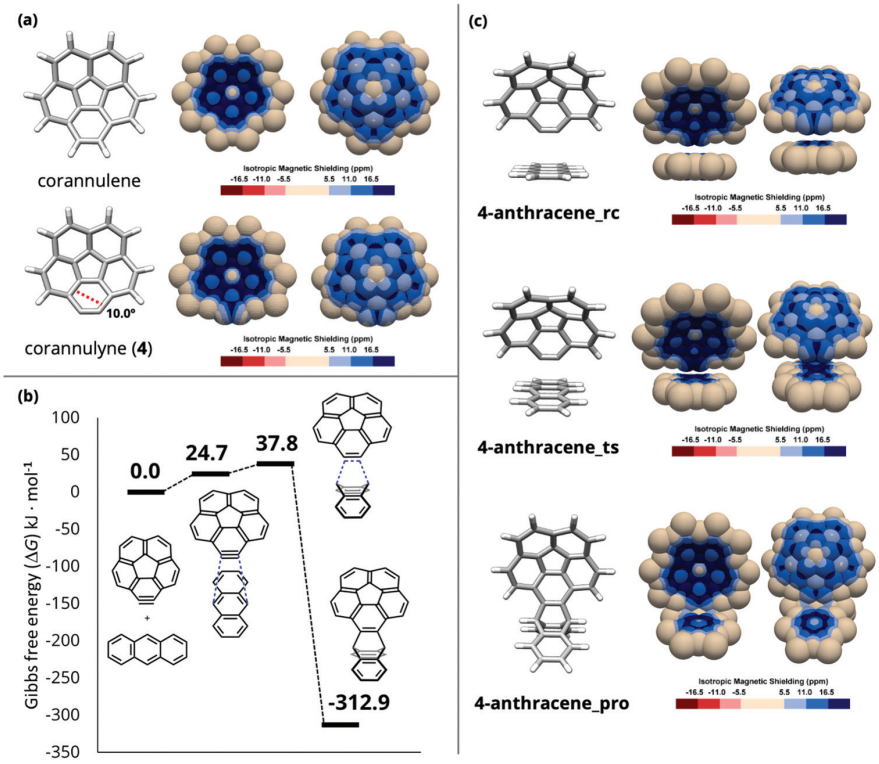

Figure 4 (a) 3D IMS contour maps of corannulene and corannulyne (**4**). (b) Gibbs free-energy profile of the [4+2] cycloaddition between corannulyne (**4**) and anthracene. Electronic energies (*E*) are provided in the Supporting Information (Figure S4). Relaxed scan between the reactant complex and the separated substrates showed the first step is a barrierless process. (c) 3D IMS contour maps of the three stationary points identified in (b).

reaction, which is clearly visible on both faces of its map (Figure 4, c). The map of **4-anthracene_pro** allows visualization of the three independent π-systems of this peculiar π-elongated triptycene derivative, as well as the differences in the electronics of their two respective faces.

In summary, multidimensional IMS contour maps were used to visualize electron delocalization and aromaticity in some selected arynes and their reactions. Benzyne (**1**), 1,2-benzo[*c*]phenanthryne (**2**), 7,8-[5]helicyne (**3**), and corannulyne (**4**) were examined. The results show that the aromatic π-system of arynes is not much affected by the reaction of their 2π-acetylenic system, even for the contorted arynes **3** and **4**. However, some trends could be identified. Arynes, planar or not, show a somewhat localized pattern at their triple bond when compared to the corresponding arenes. As a general feature, within the limits of the examined reactions, it was found that the transition states of their [4+2] cycloadditions with furan (for arynes **1** and **3**) and with anthracene (for aryne **4**), and the transition state of their annulative (2+2) dimerization (for aryne **2**), are the most aromatic species of these transformations. Overall, multidimensional IMS contour maps facilitated the analysis of electron delocalization and aromaticity in arynes and their reactions.

Conflict of Interest

The authors declare no conflict of interest.

Funding Information

This work was funded by the French Agence Nationale de la Recherche (ANR) (ANR-19-CE07-0041). Institutional financial support from Aix-Marseille University, Centrale Marseille and the Centre National de la Recherche Scientifique (CNRS) is acknowledged.

Acknowledgment

The Centre de Calcul Intensif d'Aix-Marseille is acknowledged for granting access to its high-performance computing resources.

References

(1) Takikawa, H.; Nishii, A.; Sakai, T.; Suzuki, K. *Chem. Soc. Rev.* **2018**, *47*, 8030.

(2) (a) Pozo, I.; Guitián, E.; Pérez, D.; Peña, D. *Acc. Chem. Res.* **2019**, *52*, 2472; and references cited therein. (b) Sarmah, M.; Sharma, A.; Gogoi, P. *Org. Biomol. Chem.* **2021**, *19*, 722.

(3) (a) Shi, J.; Li, L.; Li, Y. *Chem. Rev.* **2021**, *121*, 3892. (b) Fluegel, L. L.; Hoye, T. R. *Chem. Rev.* **2021**, *121*, 2413.

(4) (a) Jiao, H.; Schleyer, P. von. R.; Beno, B. R.; Houk, K. N.; Warmuth, R. *Angew. Chem. Int. Ed. Engl.* **1997**, *36*, 2761. (b) De Proft, F.; Schleyer, P. von. R.; van Lenthe, J. H.; Stahl, F.; Geerlings, P. *Chem. Eur. J.* **2002**, *8*, 3402. (c) Sánchez-Sanz, G.; Alkorta, I.; Trujillo, C.; Elguero, J. *Tetrahedron* **2012**, *68*, 6548. (d) Kleinpeter, E.; Koch, A. *Tetrahedron* **2019**, *75*, 4663.

(5) Poater, J.; Bickelhaupt, F. M.; Solà, M. *J. Phys. Chem. A* **2007**, *111*, 5063.

(6) (a) Schleyer, P. von. R.; Maerker, C.; Dransfeld, A.; Jiao, H.; van Eikema Hommes, N. J. R. *J. Am. Chem. Soc.* **1996**, *118*, 6317. (b) Schleyer, P. von. R.; Jiao, H.; van Eikema Hommes, N. J. R.; Malkin, V. G.; Malkina, O. L. *J. Am. Chem. Soc.* **1997**, *119*, 12669. (c) Gershoni-Poranne, R.; Stanger, A. *Chem. Soc. Rev.* **2015**, *44*, 6597. (d) Stanger, A. *Eur. J. Org. Chem.* **2020**, 3120.

(7) (a) Lampkin, B. J.; Karadakov, P. B.; VanVeller, B. *Angew. Chem. Int. Ed.* **2020**, *59*, 19275. (b) Karadakov, P. B.; VanVeller, B. *Chem. Commun.* **2021**, *57*, 9504.

(8) Artigas, A.; Hagebaum-Reignier, D.; Carissan, Y.; Coquerel, Y. *Chem. Sci.* **2021**, *12*, 13092.

(9) Frisch, M. J.; Trucks, G. W.; Schlegel, H. B.; Scuseria, G. E.; Robb, M. A.; Cheeseman, J. R.; Scalmani, G.; Barone, V.; Petersson, G. A.; Nakatsuji, H.; Li, X.; Caricato, M.; Marenich, A. V.; Bloino, J.; Janesko, B. G.; Gomperts, R.; Mennucci, B.; Hratchian, H. P.; Ortiz, J. V.; Izmaylov, A. F.; Sonnenberg, J. L.; Williams-Young, D.; Ding, F.; Lipparini, F.; Egidi, F.; Goings, J.; Peng, B.; Petrone, A.; Henderson, T.; Ranasinghe, D.; Zakrzewski, V. G.; Gao, J.; Rega, N.; Zheng, G.; Liang, W.; Hada, M.; Ehara, M.; Toyota, K.; Fukuda, R.; Hasegawa, J.; Ishida, M.; Nakajima, T.; Honda, Y.; Kitao, O.; Nakai, H.; Vreven, T.; Throssell, K.; Montgomery, J. A. Jr.; Peralta, J. E.; Ogliaro, F.; Bearpark, M. J.; Heyd, J. J.; Brothers, E. N.; Kudin, K. N.; Staroverov, V. N.; Keith, T. A.; Kobayashi, R.; Normand, J.; Raghavachari, K.; Rendell, A. P.; Burant, J. C.; Iyengar, S. S.; Tomasi, J.; Cossi, M.; Millam, J. M.; Klene, M.; Adamo, C.; Cammi, R.; Ochterski, J. W.; Martin, R. L.; Morokuma, K.; Farkas, O.; Foresman, J. B.; Fox, D. J. *Gaussian 16, Revision A.03*; Gaussian, Inc: Wallingford, CT, **2016**.

(10) (a) Zhao, Y.; Truhlar, D. G. *Theor. Chem. Acc.* **2008**, *120*, 215. (b) Dunning, T. H. Jr. *J. Chem. Phys.* **1989**, *90*, 1007. (c) Woon, D. E.; Dunning, T. H. Jr. *J. Chem. Phys.* **1993**, *98*, 1358.

(11) Grimme, S.; Antony, J.; Ehrlich, S.; Krieg, H. *J. Chem. Phys.* **2010**, *132*, 154104.

(12) Wolinski, K.; Hinton, J. F.; Pulay, P. *J. Am. Chem. Soc.* **1990**, *112*, 8251.

(13) Frisch, M. J.; Pople, J. A.; Binkley, J. S. *J. Chem. Phys.* **1984**, *80*, 3265.

(14) (a) Clar, E. *The Aromatic Sextet*; Wiley-Interscience: London, **1972**. (b) Solà, M. *Front. Chem.* **2013**, *1*, 22.

(15) Karadakov, P. B.; Gerratt, J.; Raos, G.; Cooper, D. L.; Raimondi, M. *Isr. J. Chem.* **1993**, *33*, 253.

(16) Arora, S.; Hoye, T. R. *Org. Lett.* **2021**, *23*, 3349.

(17) Ikawa, T.; Yamamoto, Y.; Heguri, A.; Fukumoto, Y.; Murakami, T.; Takagi, A.; Masuda, Y.; Yahata, K.; Aoyama, H.; Shigeta, Y.; Tokiwa, H.; Akai, S. *J. Am. Chem. Soc.* **2021**, *143*, 10853.

(18) Yen-Pon, E.; Buttard, F.; Frédéric, L.; Thuéry, P.; Taran, F.; Pieters, G.; Champagne, P. A.; Audisio, D. *JACS Au* **2021**, *1*, 807.

(19) (a) Hosokawa, T.; Takahashi, Y.; Matsushima, T.; Watanabe, S.; Kikkawa, S.; Azumaya, I.; Tsurusaki, A.; Kamikawa, K. *J. Am. Chem. Soc.* **2017**, *139*, 18512. (b) Yubuta, A.; Hosokawa, T.; Gon, M.; Tanaka, K.; Chujo, Y.; Tsurusaki, A.; Kamikawa, K. *J. Am. Chem. Soc.* **2020**, *142*, 10025.

(20) (a) Sygula, A.; Sygula, R.; Rabideau, P. W. *Org. Lett.* **2005**, *7*, 4999. (b) Sygula, A.; Sygula, R.; Kobryn, L. *Org. Lett.* **2008**, *10*, 3927.

(21) For 2D IMS contour maps of corannulene, see: Karadakov, P. B. *Chemistry* **2021**, *3*, 861.